Additional file 1:

Temporal variations of plume activities before the 8 October 2016 eruption of Aso volcano, Japan, detected by ground-based and satellite measurements

Masaaki Morita

Here we present supplementary information on the analysis method, results, and discussions and supplementary figures in the following pages.

1. Analysis method on satellite SO_2 mass measurements

The satellite SO_2 mass measurements in this study are based on the products provided by NASA Goddard Space Flight Center (NMSO2). The algorithm for retrieving SO_2 VCDs is based on a principal component analysis (PCA) technique (Li et al. 2013; Li et al. 2017). For the calculation of the time-averaged (10-days and monthly) SO_2 mass, we used SO_2 TRL and SO_2 PBL sub-products of the NMSO2 product. Centers of mass altitude for TRL and PBL are 0.9 km and 3 km, respectively.

The averaged SO_2 mass for TRL and PBL in certain periods (10 days and one month) were calculated following the method presented by Carn et al. (2008) and Campion (2014).

1) The daily SO_2 VCDs in each period were first gridded in a step of 0.1°, and then they were stacked and averaged by the number of days. In this procedure, pixels of the TRL and PBL sub-products with large solar zenith angle (SZA > 70°) or near the edge of the swath (rows 1–2 and 35–36) were excluded following the readme file of the NMSO2 product. Additionally, for the SO_2 PBL sub-product, only pixels with small radiative cloud fraction (RCF < 0.3) were used for the calculation.
2) The time-averaged volcanic SO_2 mass was calculated by summing the SO_2 VCDs in a volcanic region (4° in longitude×2° in latitude centered at the Aso volcano) that were higher than a threshold value (mean + standard deviation of the SO_2 VCDs in an SO_2-free region for each period). The SO_2-free region was set on the windward side of mid-latitude westerlies. These volcanic and SO_2-free regions may be affected by long-range transport of anthropogenic SO_2 from China (Kaneyasu et al. 2014). As we set the SO_2-free region here, we probably exclude the influence of anthropogenic SO_2 from China from the estimated SO_2 mass of Aso volcano to a certain degree.

The error of the SO_2 VCDs was defined as the sum of mean and standard deviation of the SO_2 VCDs in the SO_2-free region for each period. The error of the SO_2 mass shown in the results was calculated by multiplying the error of the SO_2 VCDs in each period and the area of the volcanic region. This error estimation did not include the uncertainties of the SO_2 VCDs of the original product (NMSO2), non-volcanic SO_2 from China and other regions, or volcanic SO_2 transported from nearby volcanoes (especially Sakurajima volcano). Thus, the error presented in this study is likely the minimum estimation.

2. Influence of cloud cover on satellite SO_2 mass measurements

We used the SO_2 PBL VCDs with cloud fraction (Radiative Cloud Fraction, RCF) less than 0.3 (= clear sky), therefore, basically, the SO_2 PBL mass is unlikely affected by the cloud cover. However, we used stacked VCDs to calculate the SO_2 mass, which means that, if the volcanic plume is covered with the thick cloud (e.g., in the rainy season), the averaged SO_2 mass could be underestimated. On the SO_2 TRL, we did not set the threshold for the cloud cover conditions. Thus, the SO_2 TRL mass could be much influenced by the cloud cover problem.

3. Influence of wind and atmospheric conditions on plume height

To examine the influence of wind conditions on the plume height, we made a correlation plot (Figure S1) of the plume height against the wind speed measured at the weather station (yellow triangle in Figure 1). As indicated in Figure S1, although the plume height was not larger than 200 m for large wind speed (> 10 m s^{-1}), they did not show a clear negative trend. It is difficult to completely exclude the influence of the wind speed from the plume height, but the plume height in this study was unlikely affected by the wind conditions, especially in the case of low wind speed.

We also examined the influence of atmospheric conditions on the plume height. As discussed in the Introduction, the visibility of the plume is highly affected by atmospheric conditions (Matsushima and Shinohara 2006). In a single day, vertical profiles of atmospheric temperature and humidity can vary a great deal according to the time of day. Here we made a boxplot of the plume height (Figure S2a) separated with the time of day (Figure S2b). In Figure S2b, it seems that the data have very weak semi-diurnal variations: higher values in the morning and the evening and lower values around noon. However, the amplitude of the semi-diurnal variations (e.g., the amplitude of median value for each time of day) was about several hundred meters, which was lower than the variations in the whole study period. This likely indicates that the variations of the plume height related to the volcanic activity is much higher than those related to the atmospheric conditions. In Figures S2c–h, the time-series for the limited time of day (every four hours) are shown. Although each plot does not have data for all of the study period, most plots present maxima of the plume height in a week–month scale in May–June, August, and October. They also have decreasing trends from August to October. These characteristics in Figures S2c–h are similar to those shown in Figure S2a as an envelope of the maximum plume height in a week–month scale. These results also support the conclusion above and, thus, we focus on the envelope of the maximum plume height in a week–month scale.

4. SO_2 mass vs. plume height

To examine the influence of cloud cover on the SO_2 mass, we made time-series of cloud fraction averaged in the volcanic region and the period (10-days and a month). The result is presented in Figure 5c. The time-series of monthly cloud fraction (Figure 5c) shows rough inverse correlation to that of the monthly SO_2 PBL and TRL mass (Figures 5a and S5a). However, in May and October, the SO_2 mass is lower than those of the surrounding periods even though the cloud fraction is low. Therefore, the SO_2 mass decreases in May and October seem to be relevant.

The 10-days averaged SO_2 mass (Figures 5a and S5a) does not show clear inverse correlation with the cloud fraction, especially for the PBL. However, the cloud fraction in April, mid-late June, and early September are relatively high. Thus the SO_2 mass in these periods (no. 1, 3, 8, 9, and 16 in Figures 3 and S3) may be affected by the cloud cover. This influence is also presented in Figures 5d and S5b. The points of these periods (no. 1, 3, 8, 9, and 16 in Figures 5d and S5b) are far from the fitted line, and the SO_2 mass in these periods might be overestimated (no.8) or underestimated (no. 1, 3, 9, and 16). In Figures 5d and S5b, some points plotted away from the fitted line (no. 5, 6, 12, 14, 15, 19, 20, and 21) have low cloud fraction. Thus the SO_2 mass in these periods are likely relevant. For no. 13 in Figure 3, the SO_2 VCDs in the SO_2-free region are relatively higher than those in the other period. Due to this problem, the SO_2 mass of no. 13 could be underestimated. The other points in Figures 5d and S5b are plotted near the fitted line.

5. SO_2 mass vs. SO_2 flux

The SO_2 flux data used in this study were measured by JMA. They use car traverse method to obtain the data. The traverse route is usually more than 5 km distant from the crater and, depending on the wind conditions, the plume sometimes spread over a wide area (especially for low wind speed). In high wind speed condition, the plume sometimes hugs valleys between the central cones of the volcano and, thus, the SO_2 can accumulate in the valleys. These conditions could make the SO_2 flux overestimated.

As shown in Figures 5e and S6, the SO_2 flux shows weak correlation to the 10-days averaged SO_2 mass (Figures S6a and c) but not to the monthly averaged SO_2 mass (Figures S6b and d). This difference is attributed to the temporal resolution of the SO_2 mass. In Figures S6a and c, some data are plotted to the right side of the fitted line (e.g., no. 4, 5, and 17). Although these SO_2 flux data did not have the same wind conditions (wind direction), these characteristics might be attributed to the conditions discussed above. The data no. 7 plotted in Figure S6a is in the upper side of the fitted line. This is because the SO_2 mass for this plot is likely overestimated due to the high cloud fraction (no. 8 in Figures 3 and 5d). For the data no. 10, 11, 15, and 16 in Figures S6a and c, they also plotted in the upper side of the fitted line. The SO_2 mass for these data was calculated for low cloud fraction conditions. These data were plotted far from the fitted line because of the difference in the temporal resolution between the SO_2 mass and the SO_2 flux. The other data are plotted along the fitted line.

References

Campion R (2014) New lava lake at Nyamuragira volcano revealed by combined ASTER and OMI SO_2 measurements. Geophys Res Lett 41:7485–7492. doi:10.1002/2014GL061808

Carn SA, Krueger AJ, Arellano SR, Krotkov NA, Yang K (2008) Daily monitoring of Ecuadorian volcanic degassing from space. J Volcanol Geotherm Res 176:141–150. doi:10.1016/j.jvolgeores.2008.01.029

Kaneyasu N, Yamamoto S, Sato K, Takami A, Hayashi M, Hara K, Kawamoto K, Okuda T, Hatakeyama S (2014) Impact of long-range transport of aerosols on the $PM_{2.5}$ composition at a major metropolitan area in the northern Kyushu area of Japan. Atmos Environ 97:416–425. doi:10.1016/j.atmosenv.2014.01.029

Li C, Joiner J, Krotkov NA, Bhartia PK (2013) A fast and sensitive new satellite SO_2 retrieval algorithm based on principal component analysis: Application to the ozone monitoring instrument. Geophys Res Lett 40:6314–6318. doi:10.1002/2013GL058134

Li C, Krotkov NA, Carn S, Zhang Y, Spurr RJD, Joiner J (2017) New-generation NASA Aura Ozone Monitoring Instrument (OMI) volcanic SO_2 dataset: algorithm description, initial results, and continuation with the Suomi-NPP Ozone Mapping and Profiler Suite (OMPS). Atmos Meas Tech 10:445–458. doi:10.5194/amt-10-445-2017

Matsushima N, Shinohara H (2006) Visible and invisible volcanic plumes. Geophys Res Lett 33:L24309. doi:10.1029/2006GL026506

Supplementary figures

Figure S1 Correlation plot of plume height against wind speed

Figure S2 Boxplot of plume height for each hour and time-series of plume height for every four hours

Figure S3 Maps of the 10-days averaged SO_2 TRL VCDs

Figure S4 Maps of the monthly averaged SO_2 TRL VCDs

Figure S5 Time-series of SO_2 TRL mass and its correlation plot against the fourth power of plume height

Figure S6 Correlation plot of SO_2 mass against SO_2 flux

Figure S7 Correlation plot of SO_2 mass against the fourth power of plume height with wind speed

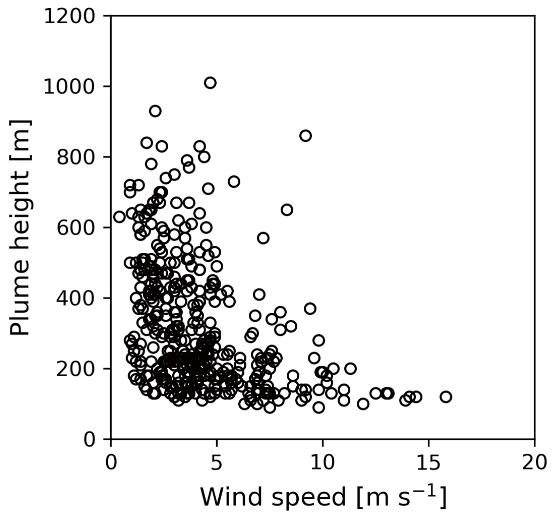

Figure S1 Correlation plot of the plume height against the wind speed measured at the weather station (yellow triangle in Figure 1)

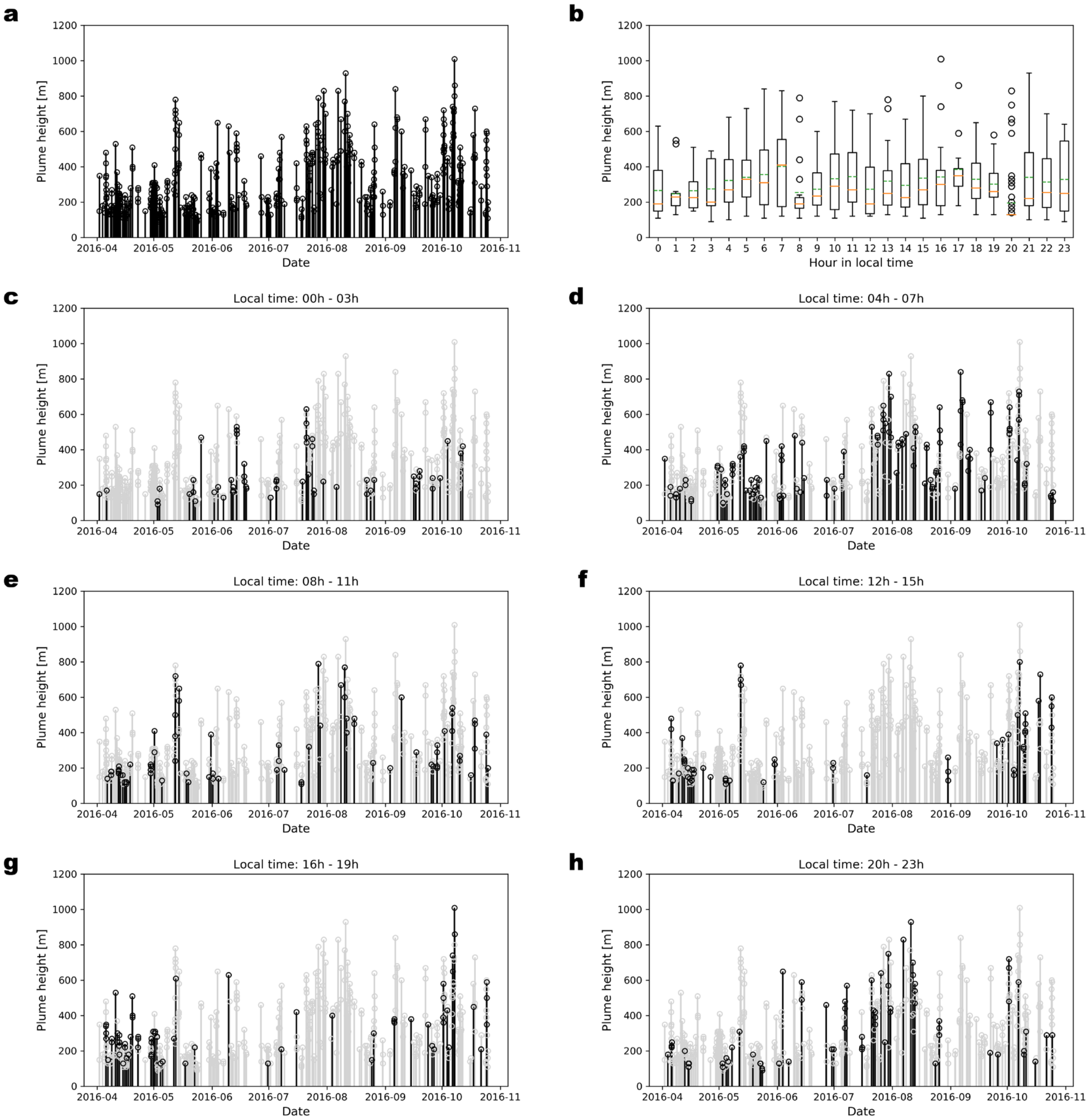

Figure S2 a Time series of the plume height estimated by the monitoring camera (as same as Figure 2). **b** Boxplot of the plume height for each hour (in local time). Orange line and green dotted line correspond to the median and mean values in each hour. **c–h** Time series of the plume height for **c** 0h–3h, **d** 4h–7h, **e** 8h–11h, **f** 12h–15h, **g** 16h–19h, and **h** 20h–23h (in local time). Gray lines correspond to the whole data shown in Figure 2 and Figure S2a.

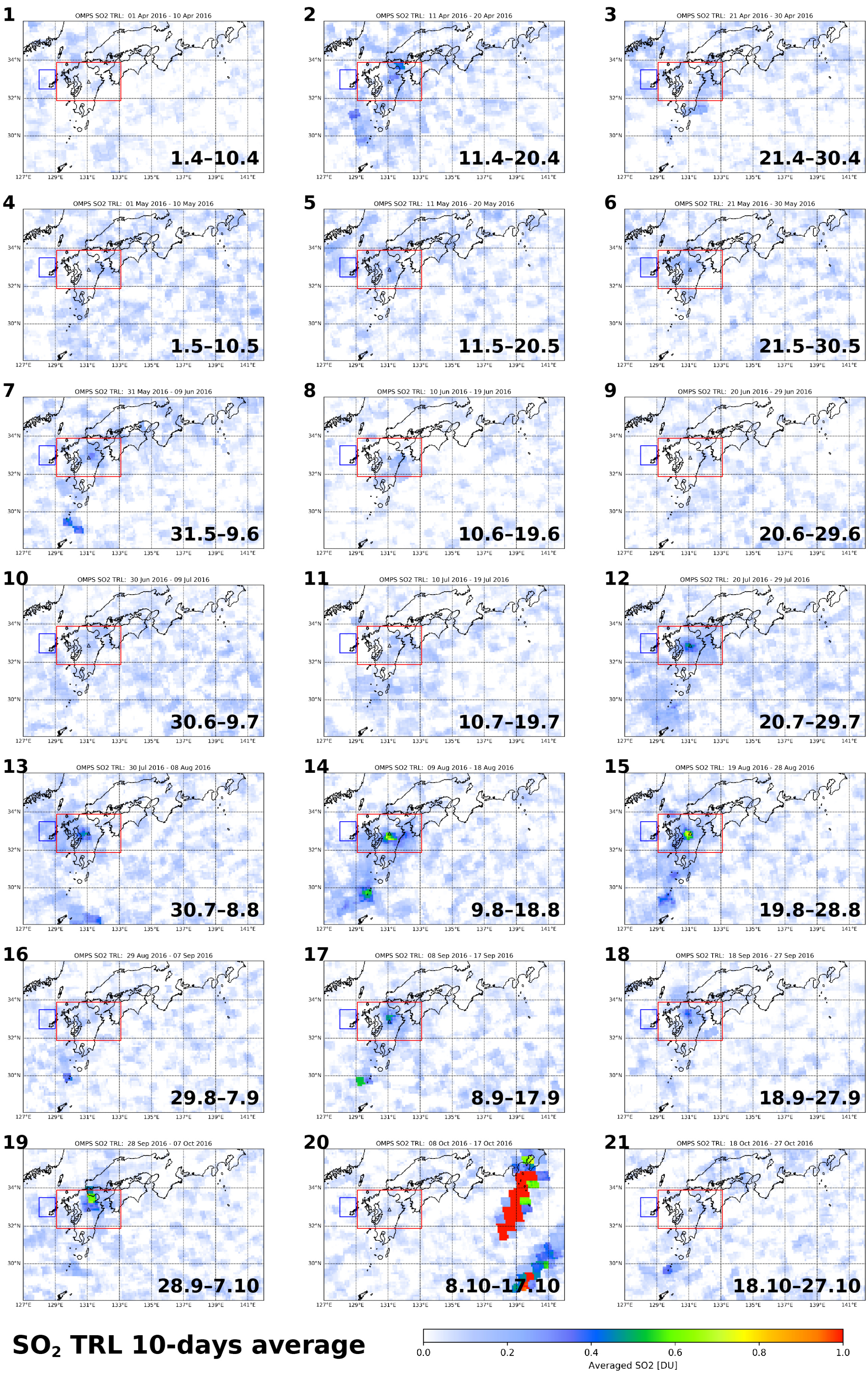

Figure S3 Maps of the 10-days averaged SO_2 TRL VCDs measured by OMPS from 1 April to

27 October 2016. The period for each map is shown in the right bottom of the map (DD.MM–DD.MM). Location of Aso volcano is depicted with the triangle. The volcanic and SO_2-free regions for the SO_2 mass calculation (see text) are shown with red and blue rectangles, respectively.

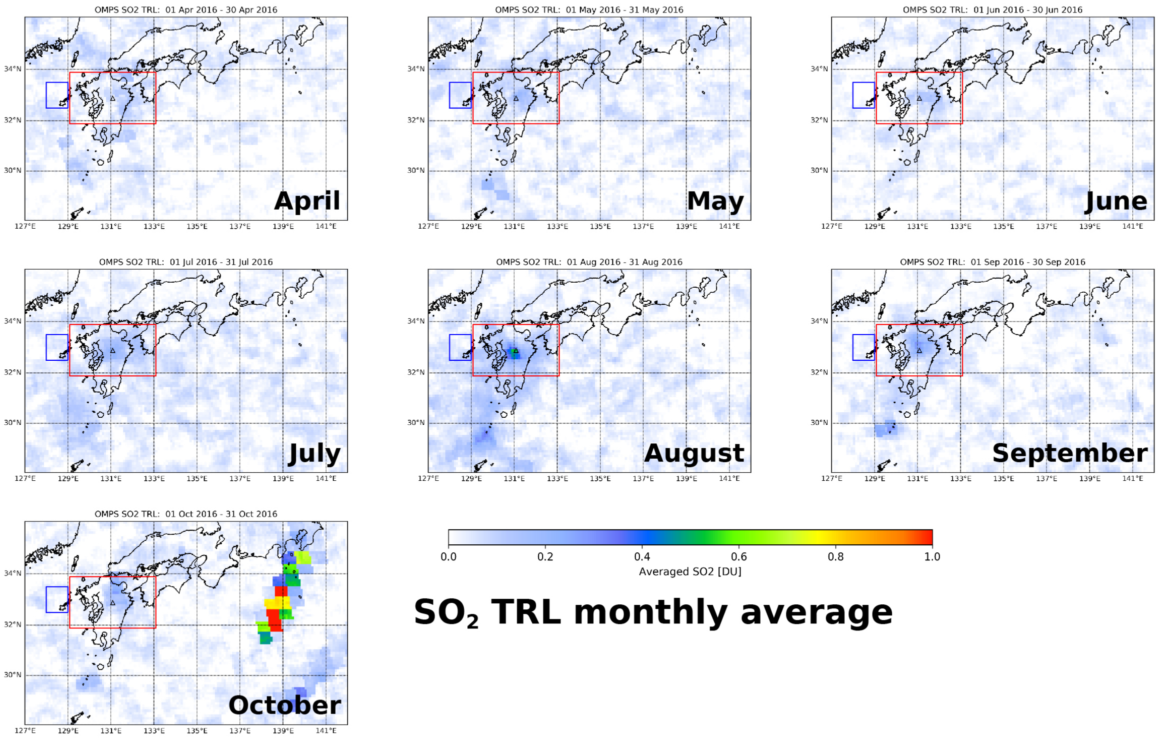

Figure S4 Maps of the monthly averaged SO_2 TRL VCDs measured by OMPS from April to October 2016. The triangle and the red and blue rectangles are as same as those in Figure S3.

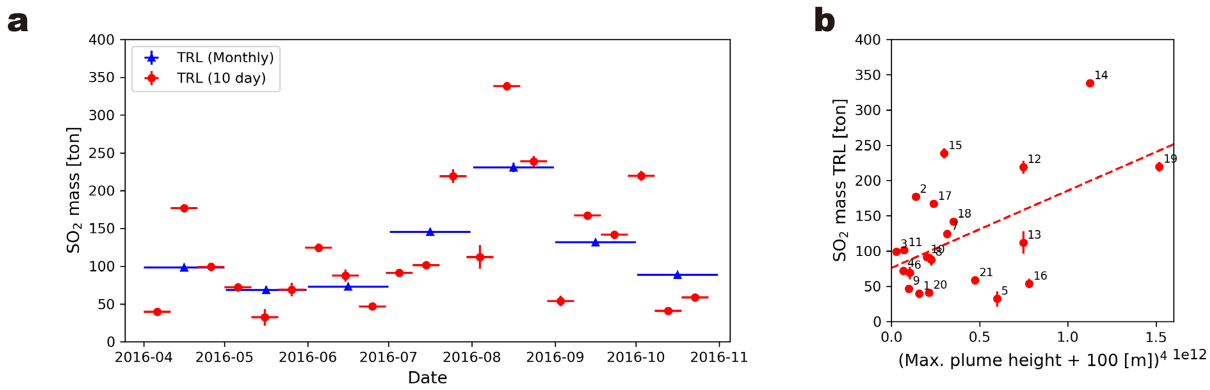

Figure S5 a The time-averaged (10-days and monthly) SO_2 TRL mass emitted by the passive degassing of Aso volcano estimated by OMPS. **b** Correlation plot of the 10-days averaged SO_2 TRL mass against the maximum plume height for the corresponding period. The plume height values are converted to those above the crater bottom (= plume height in Figure 2 + 100 m, see text). A number on the right shoulder of each point corresponds to the corresponding period number shown in Figure S3.

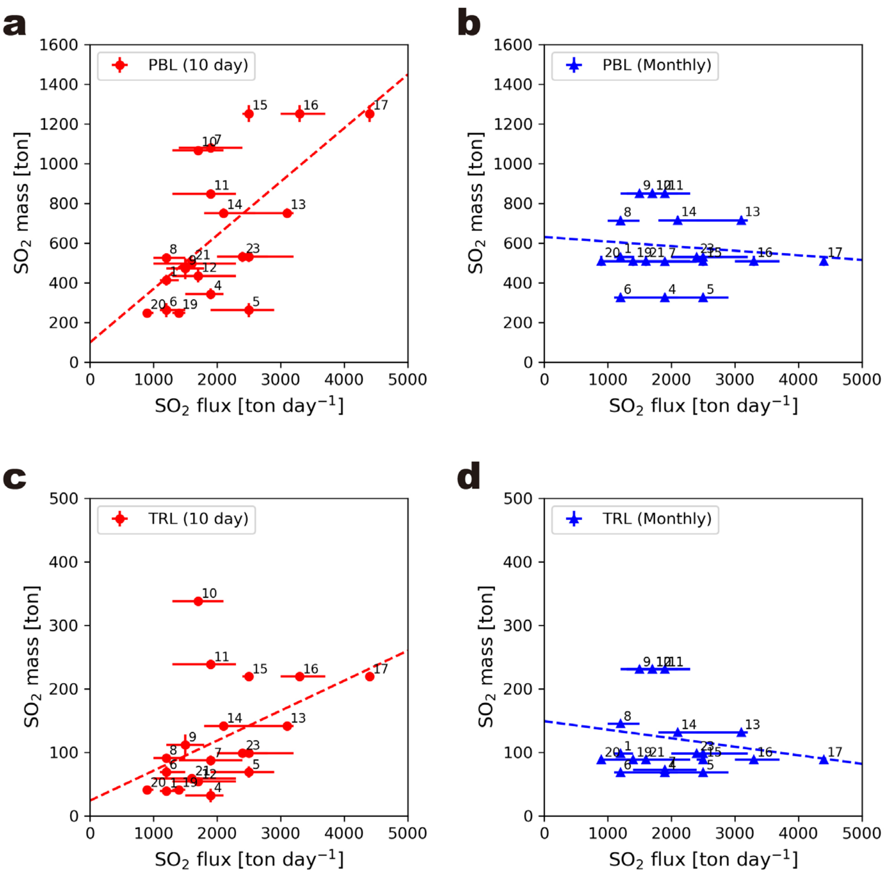

Figure S6 Correlation plot of the time-averaged SO_2 mass against the SO_2 flux for the corresponding period (**a** 10-days averaged PBL, **b** monthly averaged PBL, **c** 10-days averaged TRL, and **d** monthly averaged TRL). The SO_2 flux values are from Figure 5b but the maximum value of 15,000 ton day^{-1} measured on 7 October 2016 is not plotted here. A number on the right shoulder of each point corresponds to the corresponding SO_2 flux number shown in Figure 5b. Figure S6a is as same as Figure 5e.

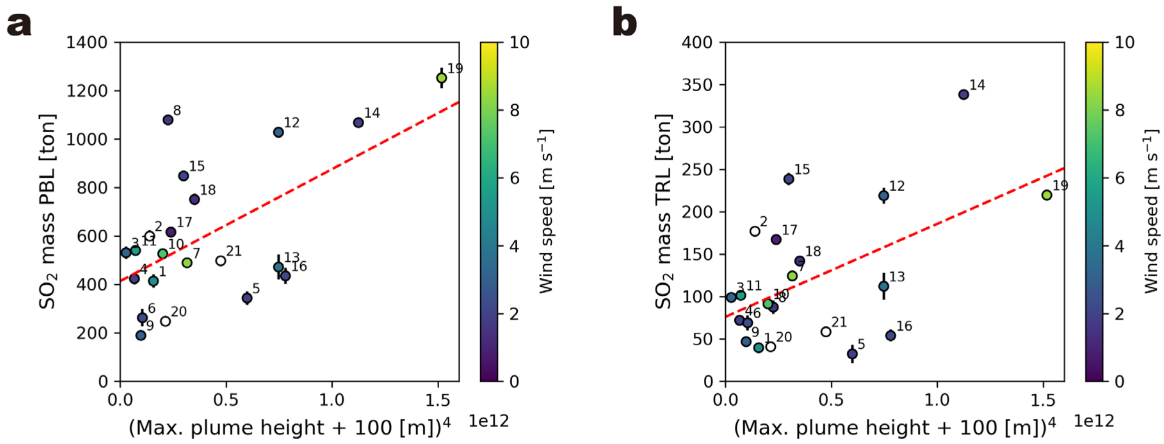

Figure S7 Correlation plot of the time-averaged (10-days and monthly) SO_2 **a** PBL and **b** TRL mass against the fourth power of the maximum plume height for the corresponding period. The plume height values are converted to those above the crater bottom (= plume height in Figure 2 + 100 m, see text). The points are colored according to the corresponding wind speed measured at the weather station (yellow triangle in Figure 1).